Research Article

Experimental Study on the Spanwise Correlation of Vortex-Induced Force Using Large-Scale Section Model

Chunguang Li ,[1] Yu Mao ,[1] Yan Han ,[1] Kai Li ,[1] and C.S. Cai [2,3]

[1]*School of Civil Engineering, Changsha University of Science & Technology, Changsha, Hunan 410114, China*
[2]*Department of Civil and Environmental Engineering, Louisiana State University, Baton Rouge, USA*
[3]*Department of Bridge Engineering, School of Transportation, Southeast University, Nanjing, Jiangsu, China*

Correspondence should be addressed to Yan Han; ce_hanyan@163.com

To investigate the spanwise correlation of vortex-induced forces (VIF) of a typical section of a streamlined box girder, wind tunnel tests of simultaneous measurement of force and displacement responses of a sectional model were conducted in a smooth flow. The spanwise correlation of VIF and pressure coefficients on the measurement points of an oscillating main deck were analyzed in both the time domain and frequency domain, respectively. The research results indicated that the spanwise correlation of VIF and pressure coefficients on the measurement points were related to the amplitudes of vortex-induced vibration (VIV), both of them weakened with the increase of spanwise distance; the maximum value of spanwise correlation coefficient is situated at the ascending stage of the lock-in region, rather than at the extreme amplitude point. The amplitudes of VIV showed different impacts on the spanwise correlation of pressure coefficients on the measurement points of the upper and lower surfaces, for which the maximum value of the spanwise correlation coefficients is located at the extreme amplitude point and the ascending stage of the lock-in region, respectively. Furthermore, the spanwise correlation of the pressure coefficients decreases continually from the upstream to downstream of the main deck; large coherence of vortex-induced forces and pressure appears around the frequency of vortex shedding, and the coherence of VIF and pressure becomes smaller with the increase in the spanwise distance.

1. Introduction

With the continuous increase in span lengths, long-span bridges are characterized by their large flexibility and low damping, and therefore more sensitive to the wind-induced vibrations, which is the primary concern for the serviceability and safety issues of the bridge. When the incoming flow passes through the main girder of long-span bridges, it is easy to produce regular vortex shedding. Once the frequency of vortex shedding is close to the frequency of the structure, it will induce structural resonance, which is known as vortex-induced vibration (VIV). VIV is a common wind-induced vibration phenomenon in long-span bridges. Although VIV has the characteristics of self-limited amplitude and will not cause destructive damage, it is prone to occur in the relatively low wind speed range, and the large vibration can cause structure fatigue damage and driving safety and even causes the public panic. VIV of field bridges

has been reported frequently. For instance, the Ishikari Kako Bridge [1], the Trans-Tokyo Bay Bridge [2] in Japan, Second Severn Bridge in Britain [3], and the Great East Belt Bridge Approach in Denmark [4] had all experienced vortex vibration to varying degrees. In 2010, the continuous box girder bridge on the Volga River in Russia experienced a severe "wavy undulation" VIV at low wind speed, with the amplitude of 40–70 cm, causing pedestrian panic. In May 2020, a large VIV also occurred on the Human Bridge in China with a single side amplitude of 31 cm. Therefore, it is of great significance to suppress VIV and explore its internal mechanism of VIF for bridge wind resistance design.

Because VIV is very sensitive to the aerodynamic configuration of the main beam, aerodynamic countermeasures are widely adopted to achieve better VIV performance due to their simplicity, reliability, and cost-effectiveness. Such applications include the guide vanes, vertical plate attached to the crash barrier, wavy railings, vertical stabilizer plate,

side plates, wind fairings, and edge plates [2, 5]. Section model wind tunnel testing is commonly used to evaluate the VIV performance of bridges and to find appropriate measures for completely eliminating or suppressing the VIV in an acceptable vibration range. However, it should be noticed that due to the inherent limitation of Reynolds number mismatch and neglect of 3D nonlinearity of the full bridge in the sectional model wind tunnel tests, the VIV prediction is not sufficiently reliable. To investigate the Reynolds number effect of the bridge section, Schewe [6] carried out tests in high-pressure wind tunnels to study the wake shape of the wing, cylinder, and bridge sections with a wide range of Reynolds numbers ($10^4 < \text{Re} > 10^7$) and concluded that the shifting of Re led to dramatic changes in the force coefficients. Using the high-pressure wind tunnel test, Schewe and Larsen [7] verified that the deviation of the VIV wind velocity between the field measurement at the Great East Belt Bridge and the wind tunnel test results is caused by Reynolds number. Scanlan and Hon [8] also emphasized that the Reynolds number effect can no longer be neglected in the wind resistance research of bridge. Therefore, it is better to use a large-scale section model to reduce the influence of Reynolds number during the section model wind tunnel tests for the bridge.

On the other hand, to overcome the shortcomings of the wind tunnel test, researchers have attempted to accurately predict the VIV of bridges through three-dimensional (3D) full-bridge analysis. In this process, the important work is to establish an accurate mathematical model of vortex-induced force (VIF). Because the VIF possesses obvious 3D features, the spanwise correlation of VIF is another critical factor for the accurate evaluation of VIV performance. In the past decades, many researchers have studied on the VIF, and a number of empirical models have been established [9–12]. However, there are relatively few works on the spanwise correlation of VIF for bridge decks. Thus, the VIF has been assumed to be well correlated in the spanwise direction. At present, an amount of research on the spanwise correlation of VIF has been carried out using a rectangular section model with different side ratios [13–17]. The aerodynamic behavior of the rectangular cylinder is controlled by its side ratio (B/D). In the ratio range of 3.5–6, the rectangular cylinders exhibit only one unsteady separation bubble and an intermittent reattached flow. Using the forced vibration device, Wilkinson [17] explored the spanwise correlation of surface pressures on a square prism. The results indicated that the spanwise correlation is incomplete and is affected by the vibration amplitude. Matsumoto et al. [14] studied the effect of different incoming flow conditions on the spanwise correlation of fluctuating pressure on 5:1 rectangular cylinders in uniform flow, turbulent flow, and 2 dimensional vertically sinusoidal flow. Liu et al. [16] found that the spanwise correlation of aerodynamic forces on the 5:1 rectangular cylinder decreases with the increase of the spanwise distance, and the correlations of fluctuating tap pressures are indeed different in the different regions of the cylinder surface. Ricciardelli [15] investigated the influence of different vibration regimes on the spanwise correlation of fluctuating pressure and VIF on the 5 : 1 rectangular cylinder

and found that the spanwise correlation increases with the vibration amplitude. In addition, the spanwise correlation of VIF and fluctuating pressure is also influenced by the DOF in which the cylinder vibrated and the excitation mechanism followed. This implies that the spanwise correlation of VIF and fluctuating pressure is different from that measured by the forced vibration test method in the wind tunnel, like the tests carried out by Wilkinson [17]. Gao and Zhu [18] have found that the forced vibration method is not suitable for measuring the fluctuating aerodynamic forces on the bridge section with a large aspect ratio because it cannot accurately simulate the two-way feedback process of fluid-structure interaction in a forced vibration test.

Compared with the rectangular cylinder, the practical streamlined box girder sections of long-span bridges often possess a larger aspect ratio even higher than 10, which means that the spanwise correlation of aerodynamic force on a streamlined box girder will be significantly different. However, the study on the spanwise correlation of VIF of bridge girders is relatively rare. Ehsan et al. [10] found that the freedom in which the structure oscillated would affect the spanwise correlation of the aerodynamic forces of the main girder with an H section shape and a side ratio of 4. Meng et al. [19] investigated the imperfect correlation of vortex-induced fluctuating pressure and the integrated vertical fluctuating force on the flat closed box deck using a large-scale section model and found that it can be greatly enhanced or changed by the deck vibration for most parts of the deck. Xu et al. [20] studied the characteristics of torsional VIV and the correlation between the surface pressure and VIF for a streamlined box girder using a small-scale section model. The results exhibited that the correlation of fluctuating pressure is relatively large along the left 1/3 and right 1/3 surface of the deck, and their contributions are great. Sun et al. [21] explored the spanwise correlation of VIF on three types of bluff body using relatively small-scale models, including a 4 : 1 rectangular cylinder, trapezoidal girder, and a typical streamlined deck. The results indicated that the largest spanwise correlation of VIF is located at the ascending stage of the VIV process rather than at the peak amplitude of vibration, and the spanwise correlation of VIF varies with the stage and amplitude of VIV. Hu et al. [22] investigated the influence of nonuniform wind field on the correlation of aerodynamic self-excited force and wind-induced response of bridges.

It is known that accurate identification of VIF and its spanwise correlation is very important for the prediction of VIV response of long-span bridges. In order to further understand the characteristics of the fluctuating VIF and surface pressures on a typical streamlined box girder of bridges, in the current study, a 1 : 25 large-scale section model was adopted in the wind tunnel test to reduce the influence of Reynolds number. The wind tunnel test was conducted using free vibration method of a spring suspension system to accurately simulate the two-way feedback process of the fluid-structure coupling during the VIV response. The vibration signal and instantaneous fluctuating wind pressure time history of the bridge deck was measured using a laser displacement sensor and simultaneous

electronic pressure scanning valve. The spanwise correlation of the total VIF and the correlation between the local pressure of individual taps and the total VIF of the section were studied. This study is helpful to deepen our understanding of the characteristics of VIF on a typical streamlined box girder for long-span bridges. Finally, some useful findings and conclusions are summarized.

2. Engineering Background

The background project is a long-span suspension bridge with a main span of 808 m in Chongqing, China. The main girder is a streamlined steel box girder with a width of 39.6 m, a height of 3.0 m, and a width to height ratio of 13.2. The upstream and downstream of the bridge deck are provided with railings, and 4 crash barriers are installed on the bridge deck. The cornerstone of the railings is a 12.5 cm concrete structure, and the maintenance tracks are arranged symmetrically at the bottom of the girder. The standard cross section of the steel box girder is shown in Figure 1.

3. Wind Tunnel Test

3.1. Experimental Setup. The section model wind tunnel test was carried out in the HD-2 boundary layer wind tunnel of the Wind Engineering Research Center of Hunan University. The size of the test section is 8 m (wide) × 2 m (high) × 15 m (long), the wind speed range of the test section is 0~12 m/s, and the turbulence intensity in the uniform flow field is less than 1%. As the VIV response is sensitive to the geometric configuration of the main girder, the detailed structure of the main girder must be simulated as true as possible. Considering the Reynolds number effect of the bridge section and other factors, the geometric scale ratio of the section model of the main girder is determined to be 1 : 25. The section model is 3.30 m long, with the width (B) of 1.58 m and a height (D) of 0.12 m. The section model skeleton is made of stainless steel frame, and the outer coat is made of high-quality wood to ensure the similarity of the geometric shape. Both end plates of the model are made of light aluminum alloy to ensure the 2D characteristics of airflow near the main girder section. The auxiliary components, such as guardrail, crash barrier, and maintenance rail, are made of plastic pipes and ABS boards, and the shape and ventilation rate of the guardrail and crash barrier are also simulated, as shown in Figure 2. The rigid section model with two degrees of freedom in the vertical and torsional direction is elastically suspended in the wind tunnel test section by 8 tension springs, and the main test parameters of the sectional model is shown in Table 1.

Five arrays of pressure taps were arranged along the spanwise direction on the model surface, as shown in Figure 3, and 53 pressure taps were arranged in each pressure measurement section, as shown in Figure 4. The arrangement of the pressure measurement section along the span can obtain a total of 9 combinations with different span distances ranging from 300 mm to 2500 mm, as shown in

Table 2. An electronic pressure scanning valve of DTC initium produced by PSI company in America is placed at each pressure measurement section inside the model, and each electronic pressure scanning has 64 channels. A plastic pressure measuring tube with a length of 1 m and an inner diameter of 1 mm is used to connect each pressure tap with the scanning valve. The plastic tubes and scanning valves were all fixed inside the model and can vibrate synchronously with the model. The sampling frequency of the electronic pressure scanning valve is 330 Hz, and the sampling time is 60 s. The time history data of the pressure of each measuring point was collected through the electronic pressure scanning valve and corrected by the frequency response function of the pressure measurement pipeline using Fourier transform. The total aerodynamic force for the whole section can be obtained by vector integration of the local aerodynamic force at all pressure taps of each pressure measurement section of the model. The aeroelastic response of the model under different wind velocities was measured by 2 laser displacement meters of optoNCDT1750 produced by Micro-Epsilon Measurement Co. Ltd in Germany. The velocity of incoming flow was recorded by the Cobra Probe produced by TFI company in Australia, and the sampling frequency is set to 500 Hz. Unfortunately, due to the different acquisition systems, the acquisition of aeroelastic response and fluctuating pressure was not fully synchronized.

In order to test the VIV performance of the original design section of the bridge, wind tunnel test was carried out in a uniform flow field, and the range of wind attack angle was 0°, ±3°, and ±5°. Test results show that there is no VIV for the original design section at an attack angle of −5°, −3°, and 0°, whereas torsion VIV occurs at an attack angle of +5° and +3°. The response amplitude exceeds the allowable value of the specification [23], and the VIV is more significant at an attack angle of +5°. Therefore, this article mainly focuses on the VIV at an attack angle of +5°.

3.2. Vortex-Induced Vibration. Due to the influence of turbulence caused by the model itself, the VIV of the section model will fluctuate in the actual wind tunnel test. Therefore, the VIV is not completely pure harmonic vibration. To more accurately calculate the vortex-induced amplitude, based on the direct amplitude given in the design specification, the root variances of vibration amplitude statistics was used to determine the VIV amplitude. The root variance of the displacement response of torsion and vertical VIV at an attack angle of +5° is shown in Figure 5. It can be seen from Figure 5(a) that the original design section produces severe torsional VIV. The torsional VIV lock-in velocity region is 6.5 m/s~9.01 m/s (corresponding velocity at the prototype bridge is 14.75 m/s~20.44 m/s), and the test velocity for the maximum amplitude is 8.5 m/s (corresponding velocity at the real bridge is 19.29 m/s). The maximum torsional amplitude is about 0.467°, which is about 2.3 times of the allowable amplitude specified in the design specification ([23] wind-resistant design specification for highway bridges, China).
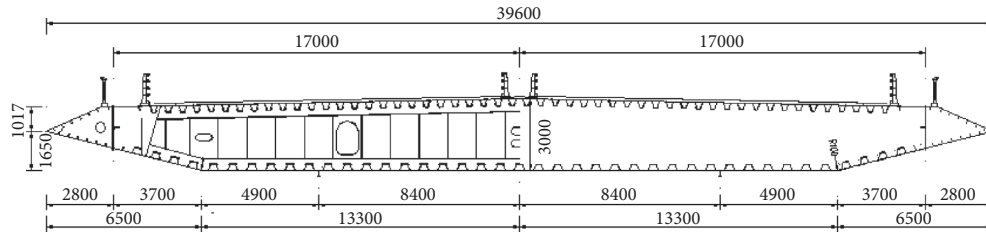
FIGURE 1: Standard cross section of steel box girder (unit: mm).

FIGURE 2: Layout of the section model wind tunnel test.

TABLE 1: Parameters of test model.

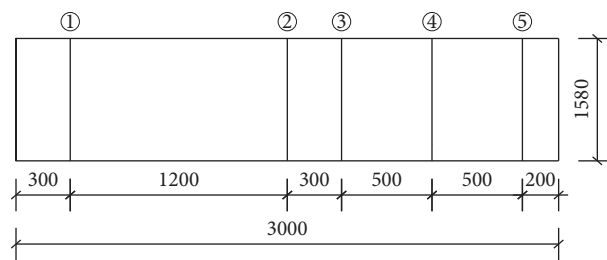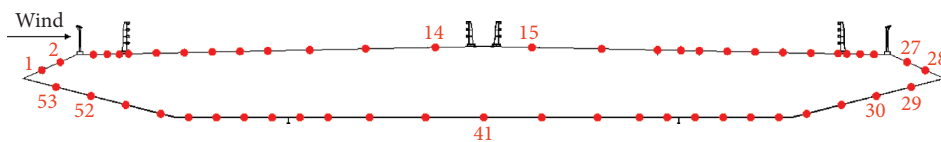| Parameter		Value of prototype bridge	Ratio of simulation	Value of model
Unit mass (kg·m^{-1})		28704	$1:25^2$	45.93
Unit mass moment of inertia (kg·m^2·m^{-1})		5784830	$1:25^4$	14.81
Frequency (Hz)	Vertical	0.1816	10.757	1.953
	Torsional	0.3895	11.032	4.297
Velocity ratio	Vertical		$1:2.32$	
	Torsional		$1:2.269$	
Damping ratio (%)	Vertical		0.48	
	Torsional		0.42	

FIGURE 3: Spanwise arrangement of pressure taps.

FIGURE 4: Arrangement of pressure taps on cross section.

As shown in Figure 5(b), the vertical VIV also occurred in the original design section with the lock-in range of 4.97 m/s to 7.1 m/s (corresponding to the wind speed at the prototype bridge of 11.35 m/s to 16.47 m/s), but the maximum amplitude of the vertical VIV was smaller than the allowable amplitude in the specification. It must be noted

TABLE 2: Combination of spanwise distance with different sections.

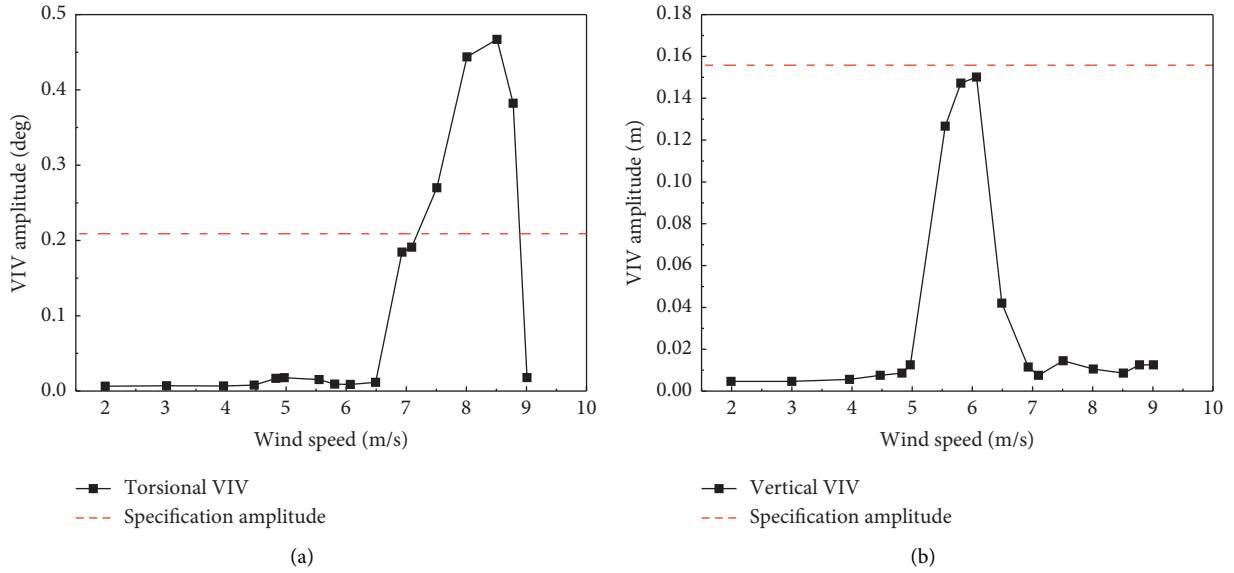| Spanwise distance δ (mm)	Dimensionless spanwise distance δ/D	Section combination
300	2.50	2–3
500	4.17	3–4
800	6.67	2–4
1000	8.33	3–5
1200	10.00	1–2
1300	10.83	2–5
1500	12.50	1–3
2000	16.67	1–4
2500	20.83	1–5

FIGURE 5: Torsional displacement response of main deck virus wind velocity. (a) Torsional VIV. (b) Vertical VIV.

that because more severe torsional VIV occurred in the original design section, and due to space limitation, only the spanwise correlation of torsional VIV was analyzed in the following paragraphs. Figure 6 shows the time-history curve and amplitude spectrum of the torque coefficient of the model under the maximum amplitude wind speed in the lock-in region of the torsional VIV. According to the amplitude spectrum of the torque coefficient, the fundamental vibration frequency of the model is 4.295 Hz, which is close to the natural frequency of the section model (4.297 Hz). However, the vibration of the model is not a harmonic vibration with a single frequency but with a second harmonic component (8.65 Hz), which reflects the nonlinear characteristics of VIF.

4. Spanwise Correlation Analysis

4.1. Definition of Spanwise Correlation Coefficient.
The spanwise correlation of VIF of the main girder section can be expressed with the spouse correlation coefficient, which is defined as follows:

$$\text{Cov}(X, Y) = \frac{\sum (X - \overline{X})(Y - \overline{Y})}{\sqrt{\sum (X - \overline{X})^2 (Y - \overline{Y})^2}}, \quad (1)$$

where X and Y are the aerodynamic parameters (such as lift, resistance, or torque) between sections at different spanwise positions. Ricciardelli [15] put forward the empirical formula of the spanwise correlation of the vibratory girder section considering the influence of self-excitation force:

$$R\left(\frac{\delta}{D}\right) = (1 - d_i)\exp\left[-c_i \frac{\delta}{D}\right] + d_i, \quad (2)$$

where δ is the spanwise distance between different sections; D is the height of the section; c_i is an exponential attenuation coefficient; d_i is the horizontal asymptotic value of the exponential attenuation function, which is shown as the completely correlated part of the aerodynamic variable, reflecting the self-excited part of the vortex-induced force; and $1/c_i$ is the spanwise correlation length, reflecting the forcing force in VIF.
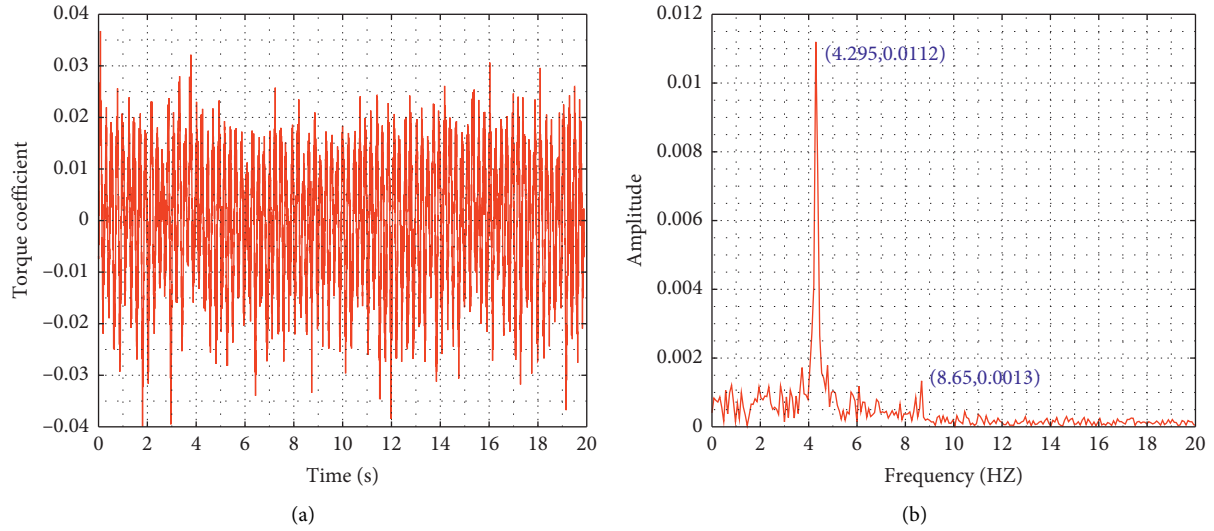
FIGURE 6: Time history and amplitude spectrum of torque coefficient. (a) Time history of torque coefficient. (b) Torque coefficient amplitude spectrum.

4.2. Spanwise Correlation of VIF. Shown in Figure 7 and Table 3 are the representative wind speeds and corresponding response amplitude selected in the torsional VIV for the spanwise correlation analysis of the VIF. Figure 8 shows the variation curve of the torque spanwise correlation coefficient with spanwise distance at different wind speeds in the lock-in region of the torsional VIV at an attack angle of +5°. From Figure 8, it can be seen that, on the whole, the spanwise correlation coefficient of the torque declines exponentially with the increase of spanwise distance and eventually tends to a fixed value that reflects a self-excited part of VIF with a complete spanwise correlation. More specifically, the spanwise correlation coefficient of the torsional torque corresponding to the starting point (V1) and ending point (V7) of the lock-in region attenuates greatly with the increase in spanwise distance. Moreover, the spanwise correlation coefficient of torsional torque at the starting point (V1) attenuates the most among the 7 representative wind speeds in the whole lock-in region. Therefore, the torsional torque spanwise correlation coefficients at the starting point (V1) and ending point (V7) are significantly smaller than those at other representative wind speed points in the lock-in region.

According to Figures 7 and 8, the spanwise correlation coefficient of the torsional torque at the ascending stage (V2–V3–V4) of the lock-in region increases with the increase in vortex vibration amplitude, and one of the interesting phenomena was observed that the spanwise correlation coefficients of the three wind speed points (V2, V3, and V4) mentioned above are all larger than that of the extreme amplitude point (V5) in the lock-in region. This result is consistent with the conclusion of Sun et al. [21]. Among them, the maximum spanwise correlation coefficient of torsional torque occurs at the third ascending point (V4) of the lock-in region, with the spanwise correlation coefficients being all above 0.8 and the maximum value reaching 0.9291, which indicates the strong spanwise correlation of
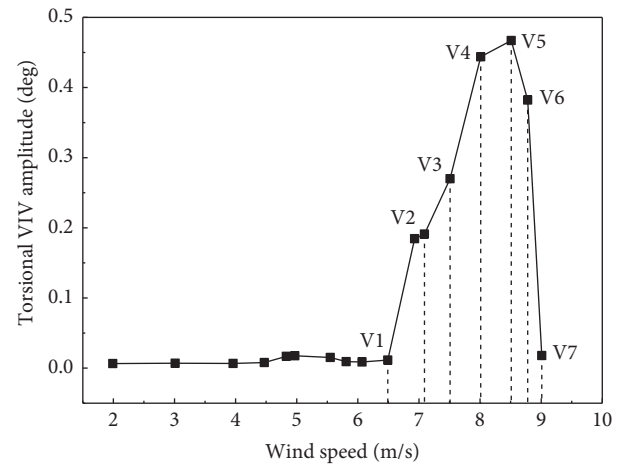

FIGURE 7: Schematic of different VIV regions and representative wind velocities.

the VIF in the lock-in region. Based on the above analysis, it can be seen that the maximum torsional torque spanwise correlation coefficient in the lock-in region is located at the third ascending point (V4), rather than at the extreme amplitude point (V5) of lock-in region.

In order to simulate the aerodynamic forces, some researchers [21, 24] assumed that the aerodynamic forces are mainly composed of two parts, one is the self-excited force related to the structural vibration and the other is caused by vortex shedding. Then the VIF can be artificially divided into vortex shedding force and self-excited force. It is known that the vortex shedding has typical three-dimensional (3D) characteristics and the 3D characteristics increase with the increase of vibration amplitude, resulting in the weakening of spanwise correlation of vortex shedding force. However, on the other hand, the self-excited force is produced by the fluid-structure coupling vibration, which has a strong spanwise correlation, and its spanwise correlation gradually

TABLE 3: Respective wind speeds selection of spanwise correlation analysis.

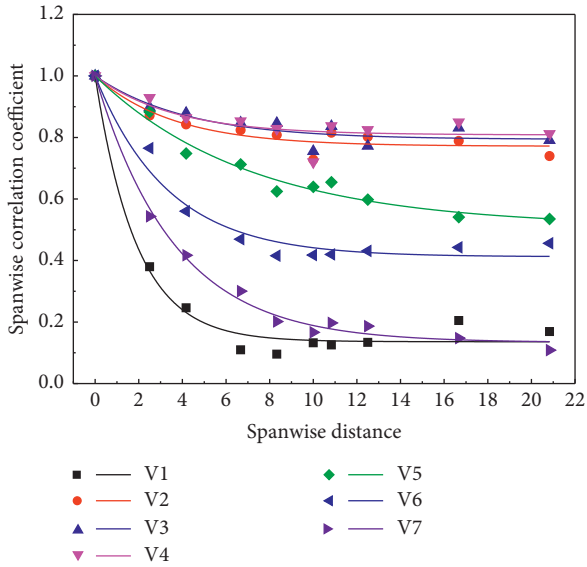| Wind speed point in lock-in region	Symbol of wind speed	Wind speed (m/s)
Starting point	V1	6.49
First ascending point	V2	7.09
Second ascending point	V3	7.51
Third ascending point	V4	8.01
Extreme amplitude point	V5	8.51
Descending point	V6	8.78
Ending point	V7	9.01

FIGURE 8: Spanwise correlation of VIF with torsional VIV.

increases with the increase of amplitude. Therefore, the VIF possess the combined characteristics of vortex shedding force and self-excited force, which explains to some extent why the maximum spanwise correlation occurs in the ascending stage rather than the position with the maximum amplitude in the lock-in stage.

Considering that the VIF of the main girder section contains components of self-excited forces in the vibratory state, the test data of VIF of the section are fitted according to equation (2). Table 4 shows the fitted parameters of the spanwise correlation coefficient of the VIF under different wind speeds in the lock-in region.

As can be seen from Table 4, the fitting parameter value c_i of the starting point (V1) in the torsional lock-in region is the largest, so the spanwise correlation of torsional torque has the largest attenuation range with the increase of the spanwise distance. On the contrary, V1 owns the minimum fitting values of d_i and $1/c_i$, and the completely correlated parts of the spanwise correlation coefficient are small. Therefore, the spanwise correlation of the torsional torque at the starting point (V1) is smaller than that of the other wind speeds in the lock-in region. The parameter fitting value d_i of the ascending stage (V2-V3-V4) of the lock-in region increases successively with the increase of the amplitude of VIV, and the completely correlated part of the torsional torque at the three points (V2, V3, V4) of the ascending stage

gradually increases. The largest parameter fitting value d_i occurs at the third ascending point (V4) in the torsional lock-in region, and the horizontal asymptotic value of the attenuation function is 0.808, indicating that the attenuation degree of spanwise correlation is very small, and the completely correlated part of the aerodynamic force is the largest. Meanwhile, the parameter fitting value of $1/c_i$, which represents the forcing force component in the aerodynamic force, is also large. Because the third ascending point (V4) is most affected by the self-excitation force and the forcing force, the torsional torque in the third ascending point (V4) of lock-in region has the greatest spanwise correlation.

4.3. Pressure Distribution Characteristics of Main Girder. Figure 9 shows the comparison of the mean pressure coefficient and standard deviations of the pressure coefficient of the five pressure measurement sections at the extreme amplitude point (V5) of the torsional vortex-locked area. In Figure 9, only the mean value of pressure coefficient and standard deviation of pressure coefficient on representative pressure taps of the 2# pressure measurement section are given. It can be seen from Figure 9(a) that the variation trend and magnitude of the mean pressure coefficient of the five pressure measurement sections are pretty close as a whole. The mean pressure coefficients of the windward oblique web on the upper surface and lower surface are large and all positive, whereas those in the leeward oblique web are small. The average pressure coefficients in the front and middle area (3#–19#pressure taps)) of the upper surface were all negative (suction). Meanwhile, it can be seen from Figure 9(b) that the standard deviations of the pressure coefficients of the five pressure measurement sections are significantly different in the middle and rear area (15#–26# pressure taps) of the upper surface, whereas in other areas of the five pressure measurement sections, the standard deviations of the pressure coefficients are generally close to each other. The largest standard deviations of pressure coefficient appeared in the middle and rear area of the upper surface of the 2# pressure measurement section, whereas that of the 3# pressure measurement section was the smallest in the same area.

Figure 10 shows the variation curve of the spanwise correlation coefficient of the representative pressure taps on the surface of the main girder with the spanwise distance under 7 representative wind speeds in the lock-in region. Three representative pressure taps were selected in the upper and lower surfaces, respectively, to analyze the spanwise correlation of pressure coefficients, including 1#, 10#, and

TABLE 4: Fitted parameters values of spanwise correlation coefficients of vortex-induced force.

| Wind speed point in lock-in region	Fitted parameter c_i	Fitted parameter d_i	Spanwise correlation length $1/c_i$
Starting point (V1)	0.530	0.136	1.887
First ascending point (V2)	0.277	0.771	3.610
Second ascending point (V3)	0.278	0.794	3.597
Third ascending point (V4)	0.275	0.808	3.636
Extreme amplitude point (V5)	0.285	0.510	3.509
Descending point (V6)	0.299	0.412	3.339
Ending point (V7)	0.375	0.134	2.667

(a)

(b)
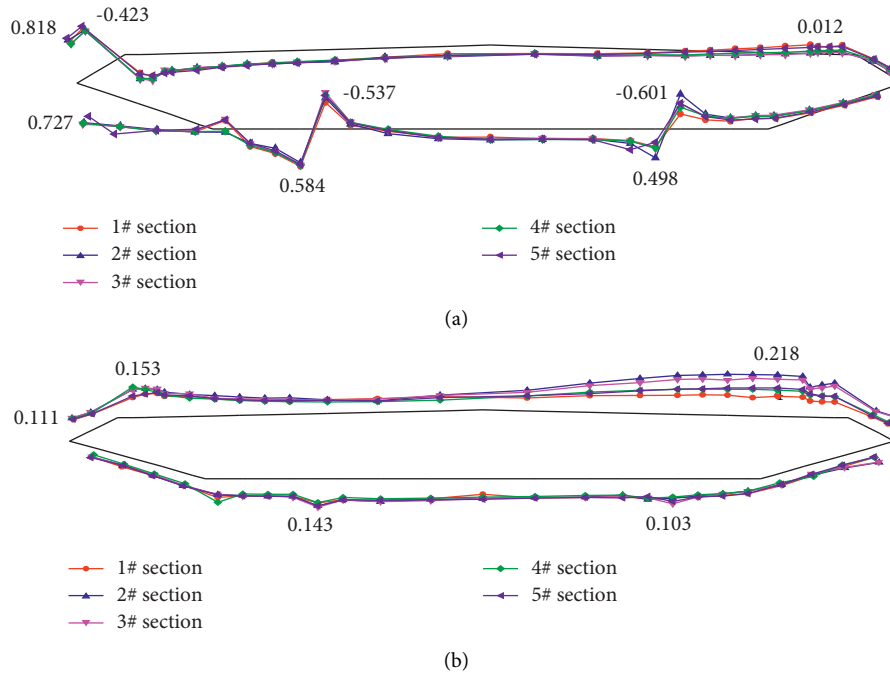
FIGURE 9: Comparison of (a) mean values and (b) standard deviations of pressure coefficient.
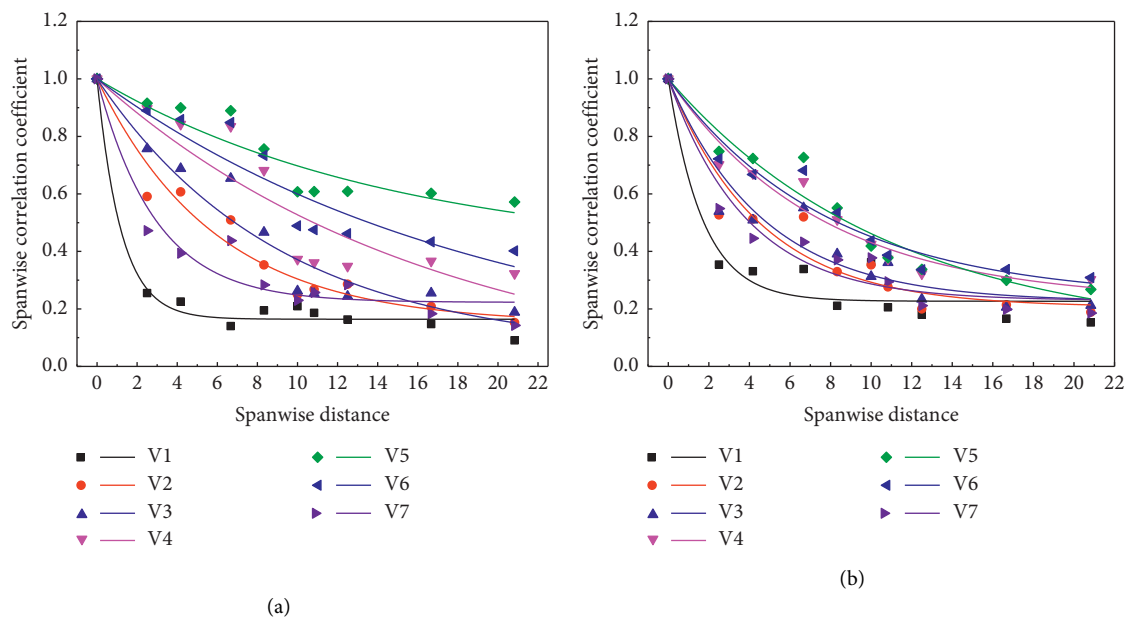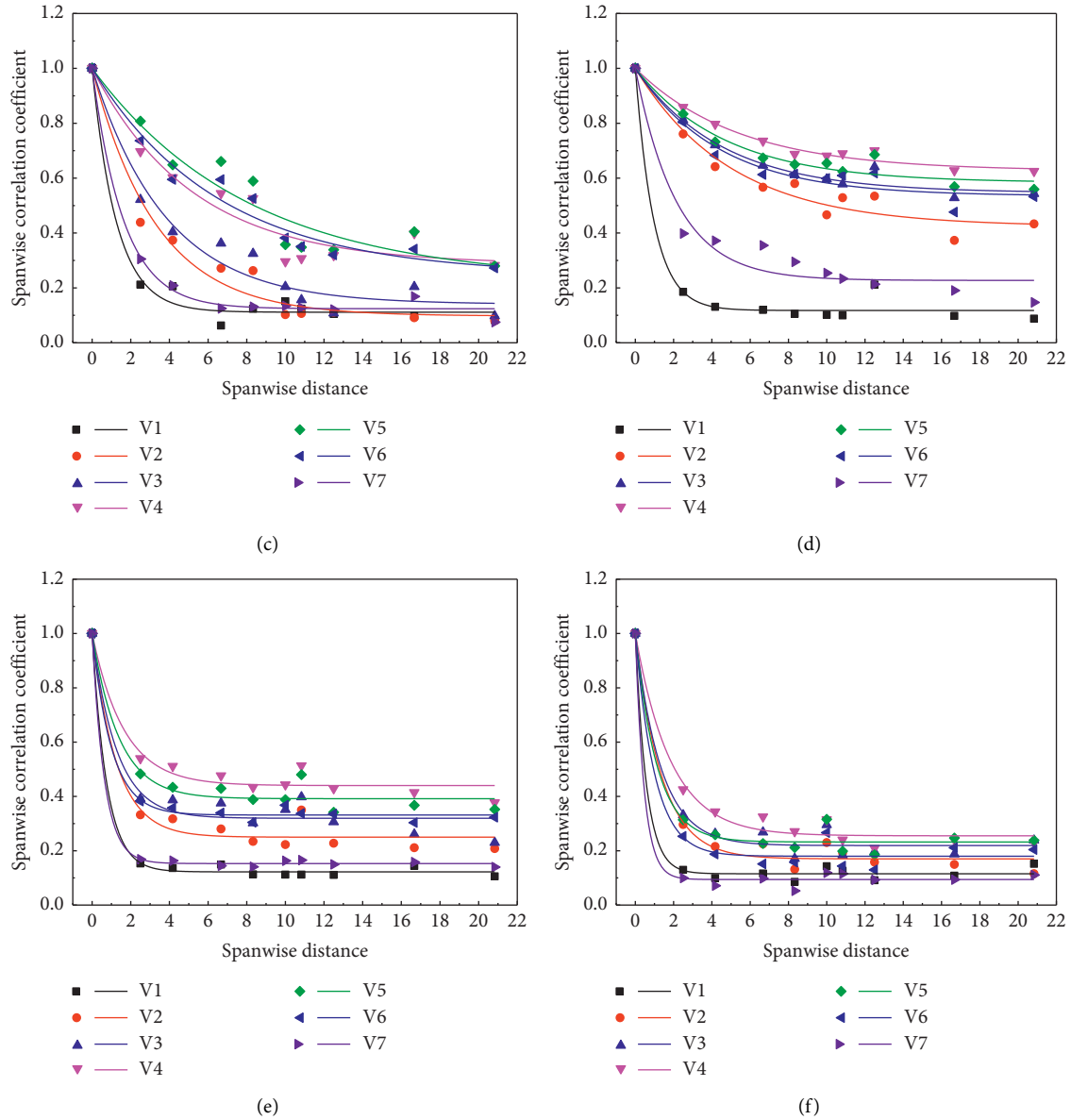

(a)

(b)

FIGURE 10: Continued.

FIGURE 10: Spanwise correlation coefficients of representative pressure taps. (a) 1# pressure measuring point. (b) 10# pressure measuring point. (c) 28# pressure measuring point. (d) 52# pressure measuring point. (e) 45# pressure measuring point. (f) 36# pressure measuring point.

28# on the upper surface and 52#, 45# and 36# on the lower surface. It can be seen from Figure 10 that the spanwise correlation coefficients of the pressure coefficients at the representing measuring points all decrease with the increase in the spanwise distance. Generally speaking, the spanwise correlation of the pressure coefficients of 1# pressure tap (on the windward oblique web of the upper surface) and 52# pressure taps (on the leeward oblique web of the lower surface) is stronger than that of other representative pressure measuring points. Among them, the spanwise correlation of pressure coefficients on both the upper and lower surfaces decreases from upstream to downstream of the section.

Figures 7 and 10 together show that the spanwise correlation of the pressure coefficient of measuring points in the lock-in region is related to the vortex vibration amplitude.

As for the representative pressure measuring points on the upper surface, the spanwise correlation of the pressure coefficient in the ascending stage (V2–V3–V4) of the lock-in region increases with the increase in vortex vibration amplitude. The maximum spanwise correlation coefficient of the pressure coefficient is located at the extreme amplitude point (V5), rather than the other representative wind speeds in the ascending stage (V2-V3-V4) of the lock-in region. The descending point (V6) has a larger spanwise correlation coefficient of the pressure coefficient than that of the other three representative wind speed points (V2, V3, and V4) in the ascending stage of the lock-in region. As for the representative pressure measuring points on the lower surface, the spanwise correlation of the pressure coefficient in the ascending stage (V2-V3-V4) of the lock-in region also
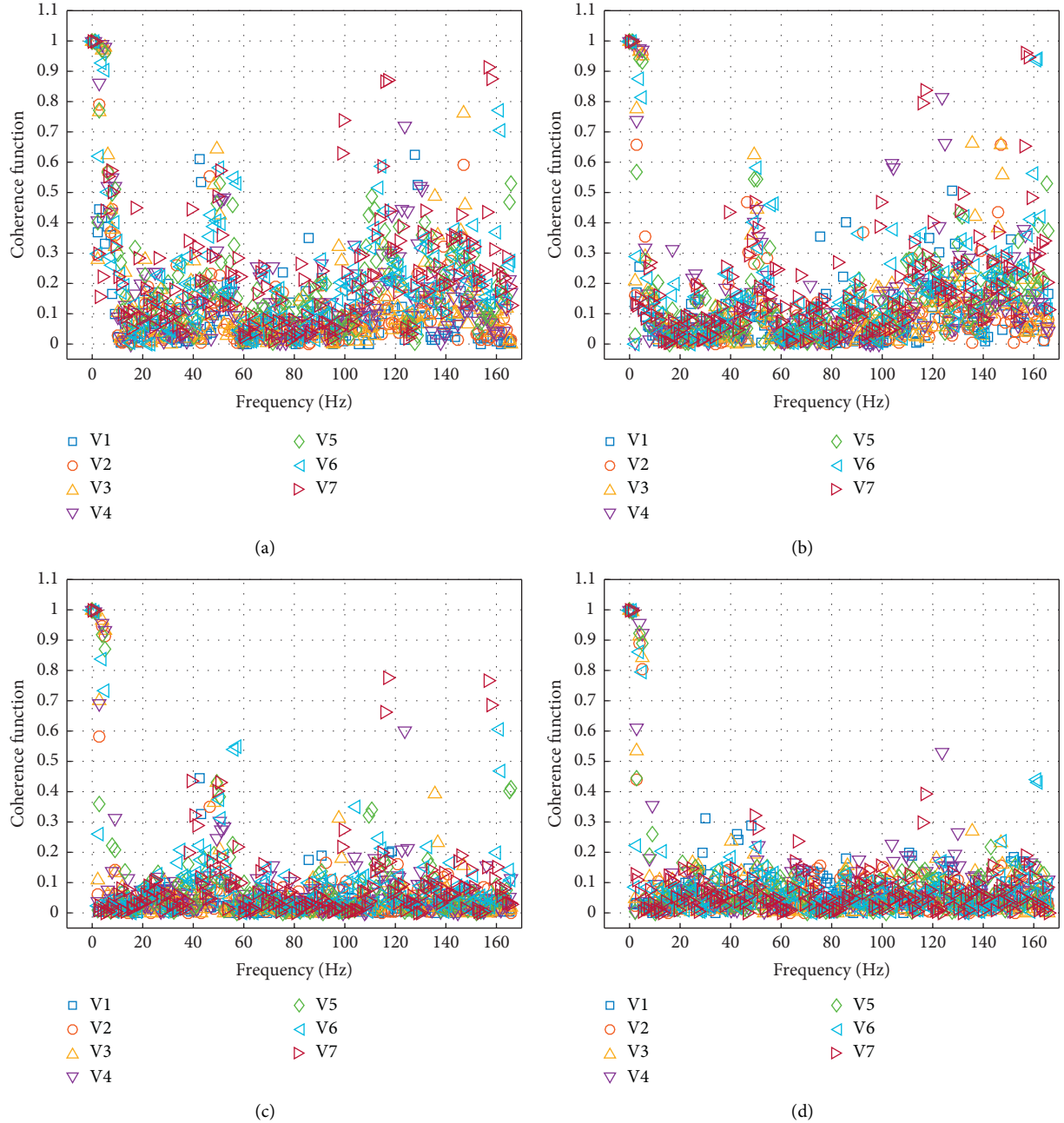
(a)

(b)

(c)

(d)

FIGURE 11: Spanwise root coherence of VIF for torsional VIV. (a) Coherence of torsion torque (3-2). (b) Coherence of torsion torque (3-4). (c) Coherence of torsion torque (3-5). (d) Coherence of torsion torque (3-1).

increases with the increase in vortex vibration amplitude. However, different from the upper surface, the maximum spanwise correlation coefficient of the pressure coefficient occurs at the third ascending point (V4), rather than at the extreme amplitude point (V5) of lock-in region. Based on the analysis above, it can be seen that the influence degree of the amplitude on the spanwise correlation of the pressure coefficient of the upper surface and the lower surface is not exactly the same.

4.4. Coherence Function of VIF. Correlation coefficient describes the degree of correlation of aerodynamic variables in

the time domain, whereas the coherence function describes the degree of correlation of the aerodynamic variables in the frequency domain. The aerodynamic coherence function between any two sections of the main girder can be defined as follows:

$$C_{XY}(f) = \frac{G_{XY}(f)}{\sqrt{G_{XX}(f)G_{YY}(f)}}, \qquad (3)$$

where $G_{XY}(f)$ is the cross-power spectral density function of aerodynamic variables between the two sections, and $G_{XX}(f)$ and $G_{YY}(f)$ are the self-power spectral density functions of aerodynamic variables.
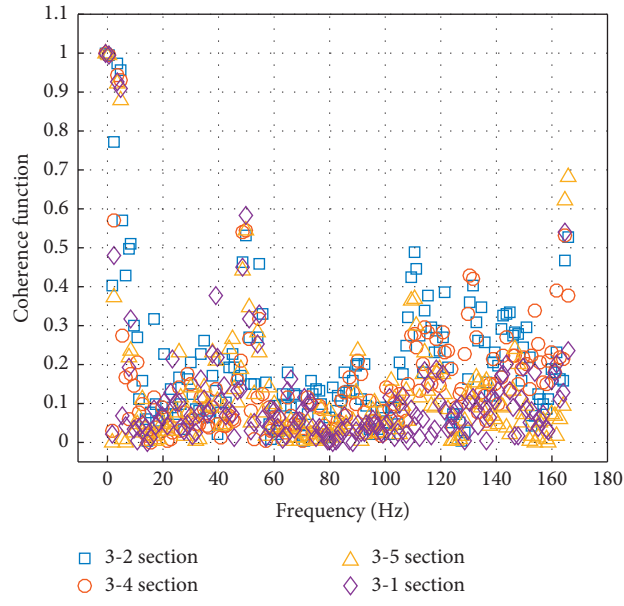
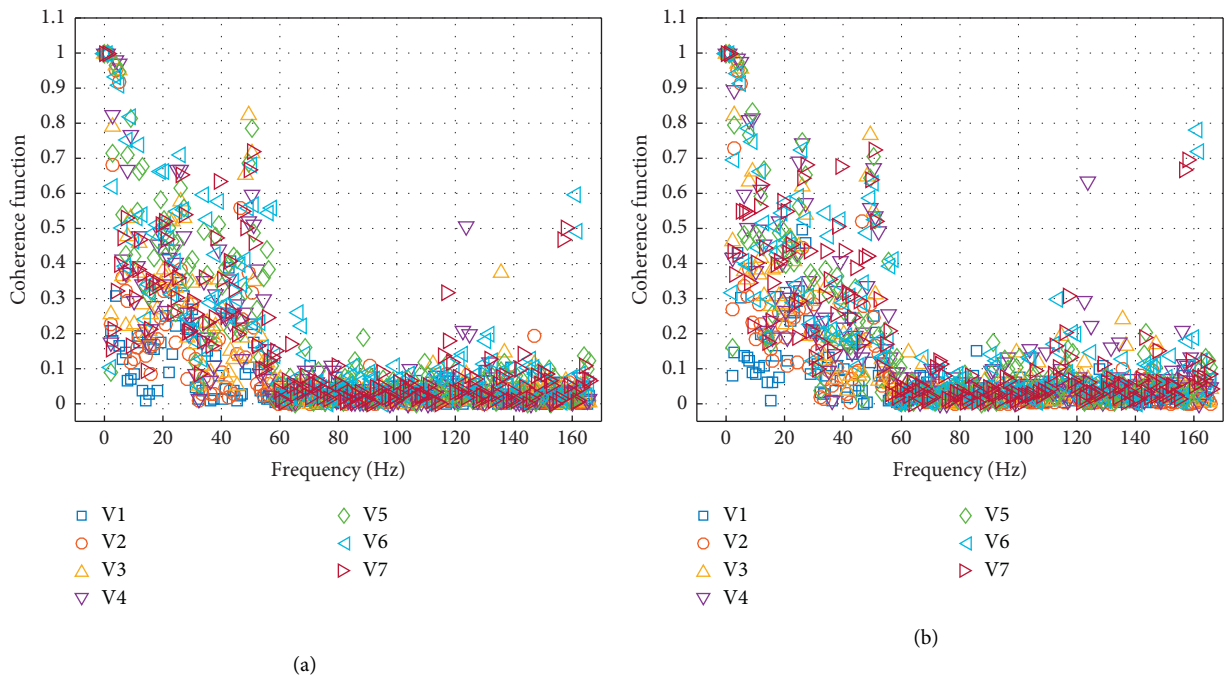FIGURE 12: Root coherence of VIF at the extreme amplitude point.
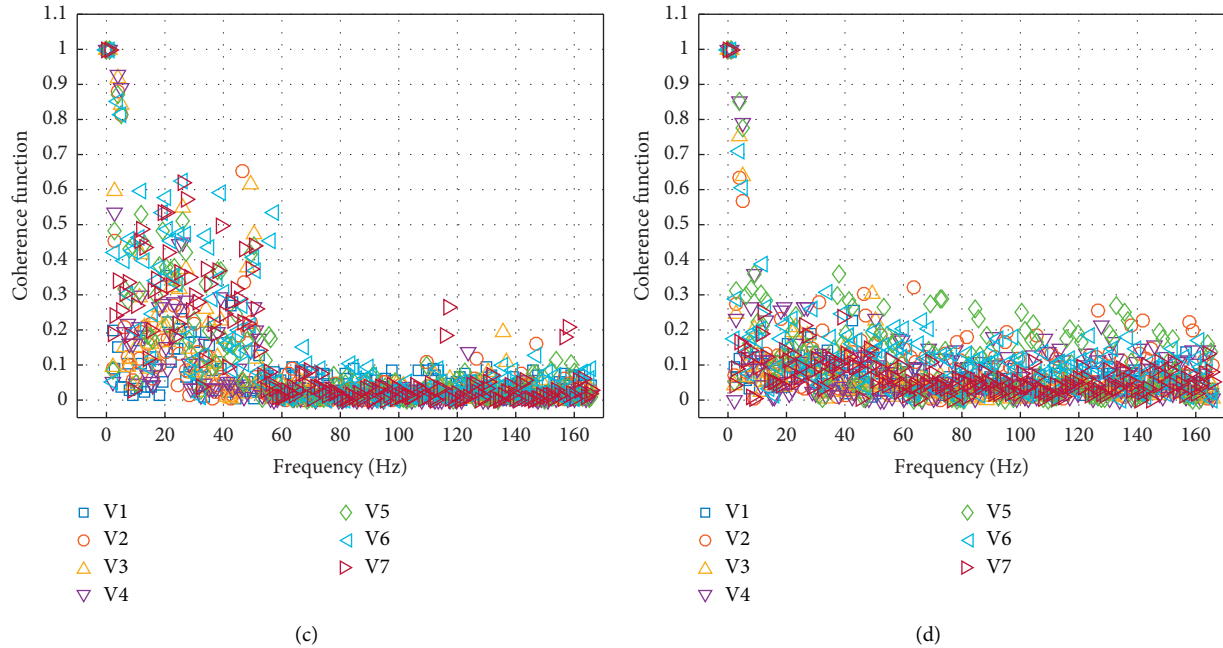

(a)

(b)

FIGURE 13: Continued.

FIGURE 13: Spanwise root coherence of representative pressure taps. (a) Coherence of pressure (3-52 with 2-52). (b) Coherence of pressure (3-52 with 4-52). (c) Coherence of pressure (3-52 with 5-52). (d) Coherence of pressure (3-52 with 1-52).

Figure 11 is the coherent function of the torsion torque between 3# section and other sections (represented by 3-1,3-2, 3-4, 3-5) in the vortex vibration lock-in region with different wind speed. As it can be seen from Figure 11, the coherence function value of the torsional torque decreases with the increase in the span distance. The coherence function of the torsional torque between 3# section and 2# section is the largest, whereas that between 3# section and 1# section is the smallest. By comparing Figures 11(a)–11(d), it can be seen that in the low-frequency range, especially near the vortex shedding frequency ($f = 4.297$ Hz), the torsional vortexes caused strong coherence. At high wind speed, the torsional vortex vibration of the main girder will be affected by self-excited vibration. As for different representative wind speed points in the vortex vibration lock-in region, multiple peaks of the coherent function appear in the high-frequency range. According to Figures 7 and 11, the coherent function value of the torsion torque at the starting point (V1) in the vortex vibration lock-in region is small, most of which are below 0.3. The coherent function value of the torsion torque at the ending point (V7) in the high-frequency range is not necessarily smaller than that of other representative wind speeds in the lock-in region. Figure 12 shows the coherent function diagram of the torsional torque between 3# section and other sections at the extreme amplitude point (V5) in the vortex-locked region, and it can be seen that the coherent function value of the torsional torque decreases with the increase in the spanwise distance.

4.5. Coherence Function of Pressure. 52# pressure tap was selected as a representative measurement point. Only the pressure coherence between 52# pressure tap in the 3# section (represented by 3–52) and 52# pressure tap in the

other four sections (represented by 1–52, 2–52, 4–52, and 5–52) was analyzed.

As it can be seen from Figure 13 that the pressure coherence of pressure 52# taps decreases gradually with the increase in the spanwise distance. The values of the pressure coherent function with different amplitudes in the lock-in region all show strong coherence in the low-frequency range, but the values of pressure coherent function decline rapidly to about 0.2 with the increase in frequency, especially in the high-frequency range. The value of pressure coherence function increases with the increase of vortex vibration amplitude in the lock-in region, which is mainly reflected in the low-frequency range. In Figure 13(d), the value of pressure coherence function in the high-frequency range is slightly larger than that in Figure 13(c). It may be because the 1# section is close to the end plate of the model, and the local turbulence around the end plate makes the pressure data of 1# section more variable.

5. Conclusions

In this study, based on the large-scale section model wind tunnel tests of a typical streamlined box girder, the spanwise correlation of VIF and surface pressure on representative pressure taps under different vibration states are studied in time domain and frequency domain, respectively, and the following conclusions are drawn:

(1) The VIF of the main girder section is not completely correlated along the span. The spanwise correlation coefficient of VIF decreases exponentially with the increase of the spanwise distance. The spanwise correlation coefficient of VIF is related to the vortex-induced amplitude. The spanwise correlation

coefficients of VIF at the starting point and ending point in the lock-in region are clearly smaller than those at the other representative wind speed points in the lock-in region. The torsional torque spanwise correlation coefficient of the ascending stage of the lock-in region increases with the increase in vortex vibration amplitude, and the spanwise correlation coefficients of the three wind speed points (V2–V4) in the ascending stage are all larger than that of the extreme amplitude point in the lock-in region (V5). The maximum spanwise correlation coefficient of torsional torque in the lock-in region is located at the third ascending point (V4), rather than at the extreme amplitude point (V5) of lock-in region.

(2) Generally speaking, for the five pressure measurement sections, the variation trend and magnitude of the mean pressure coefficient are pretty close. The standard deviations of the pressure coefficients of the five pressure measurement sections are significantly different in the middle and rear area of the upper surface, whereas in the other areas of the five pressure measurement sections, the standard deviations of the pressure coefficients are generally close to each other. The largest standard deviations of the pressure coefficient appeared in the middle and rear area of the upper surface of the 2# pressure measurement section, whereas that of the 3# pressure measurement section was the smallest in the same area.

(3) The spanwise correlation coefficients of the pressure coefficients at representing measuring points all decrease with the increase in the spanwise distance. The spanwise correlation of pressure coefficients on the upper and lower surfaces decreases from upstream to downstream of the section. It is worth noting that the spanwise correlation of the pressure coefficient of the measuring points in the lock-in region is related to the vortex vibration amplitude. However, the influence degree of amplitude on the spanwise correlation coefficient of pressure coefficient of the upper surface and the lower surface is not consistent. The maximum spanwise correlation coefficient of the pressure coefficient on the upper surface is located at the extreme amplitude point, while that of the lower surface occurs at the third ascending point of lock-in region.

(4) The coherence of pressure and VIF decreases gradually with the increase in the spanwise distance, both showing strong coherence near the vortex shedding frequency.

Data Availability

The data used to support the findings of this study are available from the corresponding author upon request.

Disclosure

Cai was formerly at Department of Civil and Environmental Engineering, Louisiana State University, Baton Rouge, USA.

Conflicts of Interest

The authors declare that there are no conflicts of interest regarding the publication of this study.

Acknowledgments

References

[1] A. R. Bureden, "Japanese cable-stayed bridge design," *Proceedings-Institution of Civil Engineers Part Design & Construction*, vol. 90, pp. 1021–1051, 1991.

[2] Y. Fujino and Y. Yoshida, "Wind-induced vibration and control of Trans-Tokyo Bay crossing bridge," *Journal of Structural Engineering*, vol. 128, no. 8, pp. 1012–1025, 2002.

[3] J. H. G. Macdonald, P. A. Irwin, and M. S. Fletcher, "Vortex-induced vibrations of the Second Severn Crossing cable-stayed bridge-full-scale and wind tunnel measurements," *Proceedings of the Institution of Civil Engineers–Structures and Buildings*, vol. 152, no. 2, pp. 123–134, 2002.

[4] A. Larsen, S. Esdahl, J. E. Andersen, and T. Vejrum, "Storebælt suspension bridge–vortex shedding excitation and mitigation by guide vanes," *Journal of Wind Engineering and Industrial Aerodynamics*, vol. 88, no. 2-3, pp. 283–296, 2000.

[5] E. Simiu and T. Miyata, *Design of Buildings and Bridges for Wind*, Wiley, New York, NY, USA, 2006.

[6] G. Schewe, "On the force fluctuations acting on a circular cylinder in crossflow from subcritical up to transcritical Reynolds numbers," *Journal of Fluid Mechanics*, vol. 133, pp. 265–285, 1983.

[7] G. Schewe and A. Larsen, "Reynolds number effects in the flow around a bluff bridge deck cross section," *Journal of Wind Engineering and Industrial Aerodynamics*, vol. 74-76, pp. 829–838, 1998.

[8] R. H. Scanlan and M. Hon, "Observations on low-speed aeroelasticity," *Journal of Engineering Mechanics*, vol. 128, no. 12, pp. 1254–1258, 2002.

[9] R. Landl, "A mathematical model for vortex-excited vibrations of bluff bodies," *Journal of Sound and Vibration*, vol. 42, no. 2, pp. 219–234, 1975.

[10] F. Ehsan, R. H. Scanlan, and H. R. Bosch, "Modeling spanwise correlation effects in the vortex-induced response of flexible bridges," *Journal of Wind Engineering and Industrial Aerodynamics*, vol. 36, no. 2, pp. 1105–1114, 1990.

[11] G. Diana, F. Cheli, and F. Resta, "Time domain aeroelastic force identification on bridge decks," in *Proceeding of the 9th International Conference on Wind Engineering*, pp. 938–949, New Delhi, India, January.

[12] E. Simiu and R. H. Scanlan, *Wind Effects on Structures: Fundamentals and Applications to Design*, John Wiley & Sons, New York, NY, USA, 3rd edition, 1996.

[13] Y. Nakamura and M. Nakashima, "Vortex excitation of prisms with elongated rectangular, H and [vdash] cross-sections," *Journal of Fluid Mechanics*, vol. 163, pp. 149–169, 1986.

[14] M. Matsumoto, H. Shirato, K. Araki, T. Haramura, and T. Hashimoto, "Spanwise coherence characteristics of surface pressure field on 2D bluff bodies," *Journal of Wind Engineering and Industrial Aerodynamics*, vol. 91, no. 1, pp. 155–163, 2003.

[15] F. Ricciardelli, "Effects of the vibration regime on the span-wise correlation of the aerodynamic forces on a 5:1 rectangular cylinder," *Journal of Wind Engineering and Industrial Aerodynamics*, vol. 98, no. 4-5, pp. 215–225, 2010.

[16] X. Liu, Y. Cui, and Q. Liu, "Wind tunnel study on spanwise correlation of aerodynamic forces on a 5:1 rectangular cylinder," in *Proceeding of the Eighth Asia-Pacific Conference on Wind Engineering*, Chennai, India, 2013.

[17] R. H. Wilkinson, "Part II: spanwise correlation and loading," *Aeronautical Quarterly*, vol. 32, no. 2, pp. 111–125, 1981.

[18] G. Gao and L. Zhu, "Measurement and verification of unsteady galloping force on a rectangular 2:1 cylinder," *Journal of Wind Engineering and Industrial Aerodynamics*, vol. 157, pp. 76–94, 2016.

[19] X.-L. Meng, L.-D. Zhu, Y.-L. Xu, and Z.-S. Guo, "Imperfect correlation of vortex-induced fluctuating pressures and vertical forces on a typical flat closed box deck," *Advances in Structural Engineering*, vol. 18, no. 10, pp. 1597–1618, 2015.

[20] F. Xu, X. Ying, Y. Li, and M. Zhang, "Experimental explorations of the torsional vortex induced vibrations of a bridge deck," *Journal of Bridge Engineering*, vol. 21, no. 12, Article ID 04016093, 2016.

[21] Y. Sun, M. Li, M. Li, and H. Liao, "Spanwise correlation of vortex-induced forces on typical bluff bodies," *Journal of Wind Engineering and Industrial Aerodynamics*, vol. 189, pp. 186–197, 2019.

[22] P. Hu, Y. Han, C. S. Cai, and W. Cheng, "Wind characteristics and flutter performance of a long-span suspension bridge located in a deep-cutting gorge," *Engineering Structures*, vol. 233, Article ID 111841, 2021.

[23] JTG/T 3360-01-2018, *Wind-Resistant Design Specification for Highway Bridges*, China Communications Press, Beijing, China, 2018, in Chinese.

[24] R. H. Scanlan, *On the State-of-the-Art Methods for Calculations of Flutter, Vortex-Induced and Buffeting Response of Bridge Structures*, Federal Highway Administration, Washington, DC, USA, FHWA-RD-80-50, 1981.